Structural Basis for Cholinergic Regulation of Neural Circuits in the Mouse Olfactory Bulb

Masakazu Hamamoto[1, 4], Emi Kiyokage[1], Jaerin Sohn[2, 3], Hiroyuki Hioki[2], Tamotsu Harada[4], and Kazunori Toida[1, 5]*

[1] Department of Anatomy, Kawasaki Medical School, Okayama, 701-0192, Japan

[2] Department of Morphological Brain Science, Graduate School of Medicine, Kyoto University, Kyoto, 606-8501, Japan

[3] Division of Cerebral Circuitry, National Institute for Physiological Sciences, Aichi, 444-8787, Japan

[4] Department of Otolaryngology, Kawasaki Medical School, Okayama, 701-0192, Japan

[5] Research Center for Ultra-High Voltage Electron Microscopy, Osaka University, Osaka, 567-0047, Japan

ABBREVIATED TITLE: Cholinergic circuits in the mouse olfactory bulb

ASSOCIATED EDITOR: Paul E. Sawchenko

INDEXING TERMS: cholinergic neuron; acetylcholine; olfactory bulb; centrifugal projection; synapse; SCR_001775; nif-0000–30467; IMSR_JAX:006410; AB_2301794; AB_2079760; AB_11180610; AB_94952; AB_2315522; AB_2187708; AB_887872; AB_572263

***CORRESPONDENCE TO:** Kazunori Toida, M.D., Ph.D.
Professor and Chairman, Department of Anatomy,
Kawasaki Medical School,
577 Matsushima, Kurashiki, Okayama, 701-0192, Japan
Phone: (+81) 86-462-1111, Fax: (+81) 86-462-1199
E-mail: toida@med.kawasaki-m.ac.jp

Grant sponsor: MEXT/JSPS KAKENHI; Grant numbers: 15K06748, 24500418, 23500419, 24500408, 15K14333, 25123709, 15H01430, 16H01426, 16H04663; Grant sponsor: Kawasaki Medical School; Grant number: 27G-4. Grant sponsor: Cooperative Study Program of National Institute for Physiological Sciences, Japan, for high voltage electron microscopy (H-1250M)

ABBREVIATIONS

AAV: adeno-associated virus

ABC: avidin-biotin peroxidase complex

ACh: acetylcholine

AON: anterior olfactory nucleus

BSA: bovine serum albumin

CLSM: confocal laser scanning microscopy

ChAT: choline acetyltransferase

DAB: 3, 3'-diaminobenzidine tetrahydrochloride

DIO: double inverted open reading frame

EM: electron microscopy

EPL: external plexiform layer

GABA: gamma-aminobutyric acid

GCL: granule cell layer

GFP: green fluorescent protein

GL: glomerular layer

HDB: horizontal limb of the diagonal band

HVEM: high-voltage electron microscopy

IPL: internal plexiform layer

-ir: immunoreactive

LM: light microscopy

MCPO: magnocellular preoptic nucleus

MTC: mitral/tufted cell

m2R: m2 muscarinic acetylcholine receptor

OB: olfactory bulb

ON: olfactory receptor neuron

palGFP: palmitoylation site-attached green fluorescent protein

PB: phosphate buffer

PBS: phosphate buffered saline

PG: periglomerular

PSD: postsynaptic density

ROD: relative optical density

TB: tris buffer

TH: tyrosine hydroxylase

VAChT: vesicular acetylcholine transporter

VGAT: vesicular GABA transporter

VGLUT3: vesicular glutamate transporter 3

WPRE: woodchuck hepatitis virus posttranscriptional regulatory element

5-HT: 5-hydroxytryptamine

ABSTRACT

Odor information is regulated by olfactory inputs, bulbar interneurons, and centrifugal inputs in the olfactory bulb (OB). Cholinergic neurons projecting from the nucleus of the horizontal limb of the diagonal band of Broca and the magnocellular preoptic nucleus are one of the primary centrifugal inputs to the OB. In this study, we focused on cholinergic regulation of the OB and analyzed neural morphology with the particular emphasis on the projection pathways of cholinergic neurons. Single cell imaging of a specific neuron within dense fibers is critical to evaluate the structure and function of the neural circuits. We labeled cholinergic neurons by infection with virus vector and then reconstructed them three-dimensionally. We also examined the ultramicrostructure of synapses by electron microscopy tomography. To further clarify the function of cholinergic neurons, we performed confocal laser scanning microscopy to investigate whether other neurotransmitters are present within cholinergic axons in the OB. Our results showed the first visualization of complete cholinergic neurons, including axons projecting to the OB, and also revealed frequent axonal branching within the OB where it innervated multiple glomeruli in different areas. Furthermore, electron tomography demonstrated that cholinergic axons formed asymmetrical synapses with a morphological variety of thicknesses of the postsynaptic density. Although we have not yet detected the presence of other neurotransmitters, the range of synaptic morphology suggests multiple modes of transmission. The present study elucidates the ways that cholinergic neurons could contribute to the elaborate mechanisms involved in olfactory processing in the OB.

INTRODUCTION

The olfactory bulb (OB) is an attractive region to study the neural organization of sensory circuits because of its distinctly laminated structure, constructed by a small number of neuron types with a diversity of chemical neuroactive substances. Sensory information is received by the odorant receptor, expressing on olfactory receptor neurons (ONs). The ONs extend their axons to olfactory glomeruli, providing input to the OB. Then the information is sent to higher brain centers via projection neurons, mitral/tufted cells, as output from the OB. In the OB, transduction of the information is regulated by both interneurons and afferent neurons (Shepherd et al., 2004). Interneurons have been well defined chemically in previous studies as has afferent regulation by ONs. Besides interneuron and centripetal regulation by ONs, centrifugal afferent fibers from other brain regions have been identified for possible modulation and processing of odor information. Three types of centrifugal inputs to the OB are well known: noradrenergic neurons from the locus coeruleus (Shipley et al., 1985), serotonergic neurons from the dorsal and median raphe nuclei (McLean and Shipley, 1987), and cholinergic neurons from the horizontal limb of the diagonal band of Broca (HDB) and magnocellular preoptic nucleus (MCPO) (Macrides et al., 1981; Carson, 1984a, 1984b; Záborszky et al., 1986, 2012). Previous studies examined the nuclei of origin of the centrifugal inputs and terminals in the OB; however, specific projection pathways and axonal tracts in the olfactory neural circuit have not yet been analyzed.

Recently, we have examined morphological features of centrifugal fibers, in particular, the serotonergic neuron at the single cell level (Suzuki et al., 2015). Single neuron tracing revealed an unexpected pattern of serotonergic axonal projection. The

serotonergic axon was distributed in multiple glomeruli in the glomerular layer (GL). A single axon formed asymmetrical synapses with a heterogeneous subpopulation of chemically distinguished interneurons in the GL. With the addition of this study, we have added to the structural analysis of centrifugal projections to the OB by analyzing the cholinergic neuron, another type of centrifugal fiber.

Acetylcholine is an essential neurotransmitter involved in various central nervous system functions such as alertness, learning, memory, arousal, and attention (Wenk, 1997; Hasselmo, 1999). Cholinergic neurons are known to have wide axonal projections to the forebrain, and the OB is one of the regions most heavily innervated (Woolf et al., 1984). In the olfactory system, the cholinergic activity has been implicated in discrimination of structurally similar odorants (Mandairon et al., 2006; Escanilla et al., 2012) and has been implicated in several types of learning such as habituation, rule learning, and perceptual learning (Fletcher and Chen, 2010).

Cholinergic neurons exert their actions through two types of transmission, synaptic and extrasynaptic transmission. Which of these modes of transmission is predominant in the olfactory neural circuits remains unknown. It is necessary to know the structure and transmission mode to understand how cholinergic neurons act on their target. A previous study using electron microscopy reported that cholinergic neurons form synapses on the dendrites of some interneurons in the rat OB, including periglomerular cells, granule cells, and superficial short axon cells (Kasa et al., 1995). Electrophysiological studies showed that cholinergic neural activity induces excitation of mitral cells (Castillo et al., 1999; D'Souza and Vijayaraghavan, 2012; Rothermel et al., 2014). However, an earlier study reported that electrical stimulation of HDB excites granule cells and thus indirectly inhibits mitral/tufted cells (MTC, Nickell and Shipley,

1988). Also, other studies indicated that cholinergic neural activity could cause both excitatory and inhibitory responses to periglomerular cells and granule cells, depending on receptor subtypes (Elaagouby et al., 1991; Castillo et al., 1999; Pignatelli and Belluzzi, 2008; Ma and Luo, 2012). The diverse effects observed by the different studies may be the evidence of much more complex circuits than previously expected.

In order to have a thorough understanding of the diverse neural activities in the OB, the projection pattern and the synaptic ultrastructure of cholinergic neurons need to be analyzed. Therefore, the aim of this study was to clarify the entire projection pathway of cholinergic neurons regulating olfactory function in the OB and to examine the detailed morphology of synapses formed by cholinergic neurons for a more thorough understanding of the regulatory mechanisms in olfactory neural circuits.

MATERIAL AND METHODS

Animals

Sixteen male C57BL/6J mice (8-16 weeks old, 20-28 g) and eleven male choline acetyltransferase (ChAT)-Cre mice (8-16 weeks old, 20-28 g) were used in this study. C57BL/6J and ChAT-Cre mice were obtained from Japan SLC, and the Jackson Laboratory (stock# 006410), respectively. Mice were kept in standard laboratory cages on a 12 hour light/dark cycle at constant temperature (24 ± 1°C). Food and water were available *ad libitum*. All animal experiments carried out in the present study were approved by the Animal Research Committee of Kawasaki Medical School (approved# 15-016, 15-029) and were conducted according to the "Guide for Care and Use of Laboratory Animals" of Kawasaki Medical School that is based on the National Institute of Health Guide for the Care and Use of Laboratory Animals (NIH publication# 80-23), revised 1996. The experiments with adeno-associated viral (AAV) vector and knock-in mice were approved by the Genetic Modification Safety Committee of Kawasaki Medical School (approved# 13-23, 14-45).

Immunocytochemistry

Eleven C57BL/6J mice were used for light microscopy (LM), correlative confocal laser scanning microscopy (CLSM), and high-voltage electron microscopy (HVEM). They were anesthetized by intraperitoneal injection of pentobarbital (0. 1 ml / 100 g body weight) and perfused transcardially with a fixative containing 4% paraformaldehyde in 0.1 M phosphate buffer (PB, pH 7.4). The brains were removed from the skull and postfixed with the same fixative for 1 hour. The brains were cut serially in 50-μm thick

parasagittal sections on a microtome (VT 1200s, Leica, Germany) and collected serially in phosphate buffered saline (PBS).

Sections were incubated with blocking solution containing 1% bovine serum albumin (BSA), 0.3% Triton X-100 and 0.5% sodium azide in PBS for 1 hour at 20 ℃ and with a mixture of goat anti-vesicular acetylcholine transporter (VAChT, 1:500, Santa Cruz, Cat# sc-7717, RRID: AB_2301794) in blocking solution for 3 days at 20 ℃. After being rinsed several times with PBS, they were incubated in biotinylated donkey anti-sheep IgG (1:200, Jackson ImmnoReserch, Cat# 713-065-147, RRID: AB_2340716) in blocking solution for 2 hours at 20 ℃ and avidin-biotin-peroxidase complex (ABC, standard variety, Vector Laboratories) diluted 1:200 in PBS for 2 hours at 20 °C. The peroxidase reaction was visualized using 0.05% 3, 3'-diaminobenzidine tetrahydrochloride (DAB, Dojindo, Japan) and 0.01% H_2O_2 in tris buffer (TB, pH 7.6) for 3-5 minutes at room temperature. After rinsing with PB, they were treated with 0.1% osmium tetroxide in 0.1 M PB for 30 minutes at 4 °C and washed with dH_2O. Finally, all sections were dehydrated through graded ethanol series, infiltrated in propylene oxide, and flat-embedded in Epon-Araldite (TAAB Laboratories, UK). Sections were analyzed by light microscopy (BX61, Olympus, Japan).

For detecting co-expression of VAChT and ChAT in the HDB/MCPO, sections were incubated in blocking solution for 1 hour at 20 ℃, and in a mixture of goat anti-VAChT (1:500, Santa Cruz) and rabbit anti-ChAT (1:5,000, Millipore, Cat# AB143, RRID: AB_2079760) for 3 days at 20 °C. After incubating in a mixture of primary antibodies, the sections were incubated in a mixture of Cy3-conjugated donkey anti-sheep IgG (1:200, Jackson ImmunoResearch, Cat# 713-165-147, RRID: AB_2315778) and FITC-conjugated donkey anti-rabbit IgG (1:200, Jackson

ImmunoResearch, Cat# 711-095-152, RRID: AB_ 2315776) for 2 hours.

For detecting contact with other specific neurons and co-expression of other neuroactive substances, the sections were incubated in blocking solution in PBS for 1 hour at 20 °C. Primary antibodies used in the present study were; 1) goat anti-VAChT (1:500, Santa Cruz); 2) rabbit anti-vesicular glutamate transporter 3 (VGLUT3) IgG (1:1,000, Synaptic Systems, Cat# 135203, RRID: AB_2187708); 3) mouse anti-vesicular gamma-aminobutyric acid (GABA) transporter (VGAT) IgG (1:5,000, Synaptic Systems, Cat#131011, RRID: AB_1966444); 4) mouse anti-tyrosine hydroxylase (TH) IgG (1:5,000, Millipore, Cat# AB318, RRID: AB_2315522); (5) rat anti-m2 muscarinic acetylcholine receptor (m2R, 1:1,000, Millipore, Cat# AB367, RRID: AB_94952). Sections were incubated in these antibodies for 4 days at 20 °C. Combinations of two or three different kinds of antibodies selected from rabbit, mouse, and rat were used for multiple immunolabeling. After incubation in mixtures of the primary antibodies, the sections were then incubated in mixtures of the following secondary antibodies for 2 h at 20 °C in blocking solution; 1) Cy3-conjugated donkey anti-sheep IgG (1:200, Jackson ImmunoResearch); 2) Alexa Fluor 647-conjugated donkey anti-mouse IgG (1:200, Jackson ImmunoResearch, Cat# 15-605-151, RRID: AB_2340863); 3) Alexa Fluor 647-conjugated donkey anti-rabbit IgG (1:200, Jackson ImmunoResearch, Cat# 11-605-152, RRID: AB_2492288); 4) FITC-conjugated donkey anti-rat IgG (1:200, Jackson ImmunoResearch, Cat# 12-095-150, RRID: AB_2340651). Sections were rinsed several times with PBS, and they were mounted on glass slides and coverslipped with VECTASHIELD mounting medium (Vector Laboratories, USA). Images were acquired with CLSM (Carl Zeiss LSM700, Germany: x40/ NA 0.95, x63/NA 1.4 plan-apochromat objective lens) with digital zoom mode.

High-voltage electron microscopy

The tissue for LM immunocytochemistry also used for the HVEM. Sections used for electron microscopy (EM) processing were cryoprotected by immersion in 30% sucrose in 0.1 M PB and freeze-thawed one or two times. Sections were pre-treated with 1% sodium tetrahydroborate in PBS for 30 minutes. In this study, we used blocking solution containing 1% BSA and sodium azide in PBS for EM. After blocking, sections were incubated in goat anti-VAChT (1:500, Santa Cruz) in blocking solution for 5 days at 20 °C. After rinsing with PBS, they were incubated with biotinylated donkey anti-sheep IgG (1:200, Jackson ImmnoReserch) and Alexa Fluor-594 FluoroNanogold-conjugated streptavidin (1:200, Nanoprobes, Cat# 7316, RRID: AB_2315780) in blocking solution for 2 hours at 20 °C. After being rinsed several times with PBS, sections were incubated in ABC (standard variety, Vector Laboratories) diluted 1:200 in PBS for 2 hours at 20 °C. After rinsing with TB, the peroxidase reaction was visualized using 0.05% DAB containing 0.01% H_2O_2, 0.02% nickel ammonium sulfate, and 0.025% cobalt chloride for 5 minutes at room temperature. The gold immunoparticle staining was improved using a silver enhancement kit (HQ silver, Nanoprobes, USA) for 4 minutes at room temperature in the dark. Sections were rinsed with PB, post-fixed with 3% glutaraldehyde in 0.1 M PB for 30 minutes, and 0.1% osmium tetroxide for 30 minutes at 4 °C. The slides were dehydrated through graded ethanol series, infiltrated in propylene oxide, and flat-embedded in Epon-Araldite. From these sections, 4-μm-thick sections were cut with an ultramicrotome, mounted on mesh grids (D-75, VECO, Holland) and examined with HVEM (Hitachi H-1250M: at the National Institute for Physiological Science, Japan) at an accelerating voltage of 1,000 kV. Stereo-paired images were prepared by tilting the specimen stages ± 8° compared to the prerecorded

images. The HVEM method in detail has been described in our previous study (Toida et al., 1998, 2002).

Viral injection

Eleven ChAT-Cre mice were used for cholinergic labeling with AAV vectors (Suzuki et al., 2015). Briefly, AAV vectors carried a system of double inverted open reading frame (DIO), palmitoylation site-attached green fluorescent protein (palGFP), and woodchuck hepatitis virus posttranscriptional regulatory element (WPRE). A production of AAV has been described in our previous study (Suzuki et al., 2015). Mice were anesthetized by intraperitoneal injection of pentobarbital (0.1 ml/100 g body weight). Then 0.5 μl of the viral vectors AAV2/1 CMV-DIO- alGFP-WPRE were injected into the HDB/MCPO (0.1 mm anterior to the bregma, ± 1.4 mm lateral to the midline, and 5.3 mm deep from the brain surface) of ChAT-Cre mice by pressure through a glass micropipette (Picospritzer Ⅲ, General Valve, USA: 10 psi, tip diameter < 33μm). These transgenic mice express Cre recombinase specifically in cholinergic neurons, and thus, only cholinergic neurons were labeled with palGFP by viral injection/infection. The AAV-injected mice were perfused seven days after injection as described above. The brains were then cut serially in 50-μm thick parasagittal sections on a microtome (VT 1200s) and collected serially in PBS.

Characterization and Visualization of GFP-expressing HDB/MCPO neurons

First, to confirm whether infected neurons co-localized with the expression of endogenous VAChT, we performed immunocytochemistry. The sections containing palGFP- ositive neurons were chosen and incubated in blocking solution containing

1% BSA, 0.3% Triton X-100, and 0.5% sodium azide in PBS for 1 hour at 20 °C. Then, they were incubated in goat anti-VAChT (1:500, Santa Cruz) in BSA for 3 days at 20 °C, and incubated in Cy3-conjugated donkey anti-sheep IgG (1:200, Jackson ImmunoResearch) for 2 hours. After specimens had been analyzed by CLSM, all serial sections were incubated in blocking solution for 1 hour at 20 °C and in chicken anti-GFP (1:10,000, Life Technologies, Cat# A10262, RRID: AB_11180610) in blocking solution three days at 20 °C. After that, they were incubated in biotinylated donkey anti-chicken IgY (1:200, Jackson ImmunoResearch Cat# 703-065-155, RRID: AB_2313596) for 2 hours, and in ABC (elite variety, Vector Laboratories) diluted 1:200 in PBS for 2 hours at 20 °C. The peroxidase reaction was visualized using DAB and 0.01% H_2O_2 in TB for 10 minutes at room temperature. After rinsing with PB, sections were treated with 0.1% osmium tetroxide in 0.1 M PB for 30 minutes at 4°C and washed with dH_2O. They were dehydrated through graded ethanol series, infiltrated in propylene oxide, and flat-embedded as described above.

Three-dimensional reconstruction of single cholinergic neurons

DAB-visualized cholinergic neurons were digitally traced and reconstructed with Neurolucida 11.0 software (MicroBrightField, USA) and a microscope (BX61, Olympus, Japan) equipped with a CCD camera (Retiga 2000R, QImaging, Canada).

Electron microscopy and electron tomography

Five C57BL/6J mice were used for electron microscopy (EM). They were anesthetized by intraperitoneal injection of pentobarbital (0. 1ml/100 g body weight) and perfused transcardially with a fixative containing 4% paraformaldehyde and 0.05%

glutaraldehyde in 0.1 M PB. The OBs were cut serially in 50-μm thick coronal sections. After blocking, sections were incubated with; 1) goat anti-VAChT antibody (1:500, Santa Cruz); 2) rabbit anti-5 hydroxytryptamine (HT) IgG (1:50,000, ImmunoStar, Cat# 20080 RRID: AB_572263) in blocking solution for 5 days at 20 ℃. After being rinsed several times with PBS, they were incubated in; 1) biotinylated donkey anti-sheep IgG (1:200, Jackson ImmnoReserch); and 2) biotinylated horse anti-rabbit IgG (1:200, Vector Laboratories, Cat# BA1100 RRID: AB_2336201) in blocking solution for 2 hours at 20 ℃ and ABC diluted 1:200 in PBS for 2 hours at 20 ℃. The peroxidase reaction was visualized using DAB and 0.01% H2O2 in TB for 3-5 minutes at room temperature. The sections were treated with 1% osmium tetroxide in 0.1 M PB for 1 hour at 4 ℃ and then washed with dH_2O. They were treated with 2% aqueous uranyl acetate for 30 minutes 4 ℃ and washed with dH_2O. The sections were dehydrated through graded ethanol series, infiltrated in propylene oxide, and flat-embedded in Epon-Araldite. From these samples, thin sections 75-80 nm in thickness were cut with an ultramicrotome (Reichert-Nissei Ultra-Cuts, Leica, Germany) and examined with a digital transmission EM (JEM-1400, JEOL, Japan). Each synapse was analyzed with electron tomography to examine fine synaptic structures in more detail. Tilt series were recorded with the TEM recorder (Ver. 2.32, JEOL) from +60° to -40° with 1° steps and reconstructed by tomography (TEMography software, Ver. 2.7, System In Frontier, Japan). Composer software (Ver. 3.0, System In Frontier) and Visualizer-kai software (ver. 1.5, System In Frontier) were also used to display reconstruction data. Thus, 360° rotation by 1° step and 0.5 nm step reslice images could be obtained from three-dimensional (3D) voxel data. Immuno-EM methods and electron tomography methods have been described in our previous study (Toida et al., 1998, 2000; Suzuki et

al., 2015).

Image analyses

VAChT immunoreactive (-ir) axons were reconstructed with Neurolucida 11.0 software (MicroBrightField) and a microscope (BX61, Olympus) equipped with a CCD camera (Retiga 2000R, QImaging). The digital images were taken from five random OB areas. Image J software (National Institutes of Health, USA) was used to calculate the integrated optical density of each image as a relative optical density (ROD) = log (256/mean gray level), and this was normalized to the ROD of the external plexiform layer (EPL). The length, the number of varicosities and branching point from digital reconstruction data for LM were measured with Neurolucida Explorer 11.0 software (MicroBrightField). Synaptic components of cholinergic, serotonergic neurons and olfactory receptor neurons were measured with the scale bar of the EM images.

Statistical analysis

The density of varicosities of cholinergic neurons, and the number of varicosities per length on a 3D-traced fiber among the layers were assessed using a student's *t*-test. Differences in thickness of postsynaptic density (PSD) of cholinergic neurons and other neurons in the GL were evaluated using Z-tests, student's *t*-tests, and the Welch test. Differences were considered statistically significant at $p < 0.05$. Statistical analysis was performed using StatMate IV software (ATMS, Japan). Mean ± standard error of the mean was used throughout the text of central tendency and dispersion measure, respectively.

Characterization of primary antibodies

All primary antibodies used in this study were listed in Table 1. These antibodies have been characterized and used in previous studies.

A goat anti-VAChT antibody was produced against a peptide at the N-terminals of VAChT of human origin (amino acids 1-33). The antibody detected a single band at 70KDa on Western blot analysis from mouse brain (manufacturer's data sheet at www.scbt.com). The staining pattern identified by this antibody was identical to previous reports of cholinergic soma and fibers in the mouse brain (Tsutsumi et al., 2007).

A rabbit anti-ChAT antibody recognized human placental enzyme as the immunogen. The antibody precipitated a 68 kDa band on Western blots from human brain and placental cells (manufacturer's data sheet at www.millipore.com). This antibody has been previously characterized, and the pattern of distribution was consistent with the description of the ChAT immunoreactivity in a previous study (Hassani et al., 2009).

A chicken anti-GFP antibody was raised against GFP isolated directly from jellyfish *Aequorea Victoria*, and the IgY fraction was purified by affinity purification. The antibody recognized purified GFP consisting of 238 amino acids at 27 kDa and detected precise expression of the monitoring gene (Takashima et al., 2007).

A mouse anti-VGAT antibody raised against amino acids 75-87 of rat VGAT labels a single band of 57 kDa in blots of rat brain (Takamori et al., 2000) and mouse retina (Guo et al., 2009). The immunostaining pattern of this antibody strongly correlated with glutamic acid decarboxylase (GAD) immunostaining pattern (Micheva et al., 2010).

A rabbit anti-VGLUT3 antibody recognized recombinant C-terminals of mouse VGLUT3 (amino acids 543-601) as the immunogen. The antibody recognized the band of around 60 kDa on Western blot analysis from synaptic vesicle fraction of mouse brain

(manufacturer's data sheet at www.sysy.com). VGLUT3 is expressed in glutamatergic, GABAergic (Fremeau et al., 2002), cholinergic (Gras et al., 2002), and serotonergic neurons (Hioki et al., 2010) in many parts of the nervous system. The staining pattern in the mouse OB was similar to that previously reported (Tatti et al., 2014).

A rat anti-m2R antibody was produced against the i3 loop of the human m2 receptor fusion protein (amino acids 225-359) with Glutathione S-transferase (GST). This antibody recognized a single band on Western blots corresponding to the m2i3-GST fusion protein (Levey et al., 1995). No immunoreactivity with this antibody was observed in m2 receptor knockout mice (Jositsch et al., 2009). The antibody stains striatal interneurons, including cholinergic and somatostatin-neuropeptide Y interneurons in the rat striatum (Bernard et al., 1998). The pattern of immunoreactivity of m2R in the OB was similar to that seen in a previous study (Crespo et al., 2000).

A mouse anti-TH antibody was raised against TH purified from rat PC12 cells and recognized an epitope on the outside of the regulatory N-terminus and a protein of approximately 60 kDa on Western blot analysis from brain sympathetic nerve terminals and adrenal glands (manufacturer's data sheet at www.millipore.com). Specificity was further confirmed by cell morphology consistent with previous reports (Collier et al., 1999).

A rabbit serotonin (5-hydroxytryptamine: 5-HT) antibody was raised against paraformaldehyde-coupled conjugates of BSA and 5-HT (manufacturer's data sheet at www.immunostar.com). The immunostaining pattern was consistent with a thorough description of the 5-HT immunoreactivity in a previous study (Bregman, 1987).

RESULTS

Distribution of cholinergic neurons in the OB

In this study, allocation of cholinergic neurons in the olfactory neural circuits was analyzed by immunocytochemistry using an anti-VAChT antibody. Although antibodies against ChAT have often been used to identify cholinergic neurons, recently, an anti-VAChT antibody has also been used as a selective marker for cholinergic neurons. It clearly immunolabels the axons, the dendrites, and somata of the neurons (Gilmor et al., 1996; Ichikawa et al., 1997). Thus, we used anti-VAChT to label cholinergic neurons in the present study and found that VAChT-ir fibers distributed throughout all brain regions (Fig. 1A). The highest immunoreactivity was observed in the HDB/MCPO, the nuclei of origin of cholinergic neurons that projects to the OB (Fig. 1B). These neurons were double-immunoreactive for anti-VAChT and anti-ChAT, and these two markers co-localized in the same cells (Fig. 1C). Moderate immunoreactivity for VAChT was observed in the OB, and VAChT-ir fibers were found throughout all layers. (Fig. 1A and D). No VAChT-ir somata were located in the OB (Fig. 1D-F). The highest density of VAChT-ir fibers was found in the GL and internal plexiform layer (IPL, Fig. 1D). Our results correspond well to those by previous immunocytochemical reports using other cholinergic markers and the results from OB of other species (Carson and Burd, 1980; Liberia et al., 2015). In the GL, VAChT-ir fibers were distributed both in the periglomerular and the intraglomerular regions. Many fibers were tortuous and intermingled in the GL and the IPL so that it was difficult to identify individual fibers. In the EPL, although the majority of VAChT-ir fibers ascended vertically from the granule cell layer (GCL) to the GL, some fibers exhibited little branching and ran parallel to the

layer. In the GCL, branching and various tracts of VAChT-ir fibers were observed running parallel and vertical to the layer. To clarify fine morphology of the VAChT-ir fibers with particular reference to ultrastructural features at varicose portions, we conducted HVEM examinations. HVEM images clearly revealed varicosities and non-varicosity portions of cholinergic axons with extra morphometry diameters which were 0.81 ± 0.031 μm and 0.25 ± 0.033 μm, respectively (Fig. 1E and F). There were statistical differences in the densities of VAChT-ir fibers (ROD ratio) between layers (ON= 0.35 ± 0.14, GL= 3.44 ± 1.27, EPL= 1, MCL= 1.66 ± 0.59, IPL= 4.27 ± 1.81, GCL= 1.89 ± 0.83: GL vs. EPL; $p < 0.05$, IPL vs. EPL; $p < 0.05$, ON vs. EPL; $p < 0.01$, Fig. 1G).

A single cholinergic neuron traced from HDB/MCPO to the OB

AAV was injected into the HDB/MCPO of ChAT-Cre mice for selective labeling of cholinergic axons in the OB. We confirmed that all of the infected neurons in the HDB/MCPO were cholinergic neurons by immunofluorescence staining (Fig. 2A). The density of infected axons was similar to that seen when immunostaining for VAChT using wild-type mice (Fig. 1D). The highest density of cholinergic axons in the OB was observed in the GL (Fig. 2C) where many axons crossed into adjacent glomeruli (Fig. 2D). A moderate density of axons was found in the GCL (Fig. 2F), most of which had multiple branches and extended to various regions of the GCL. In the EPL, some axons ascended into multiple glomeruli (Fig. 2E).

Because cholinergic axons have tortuous courses and numerous branches within the OB, we traced a single cholinergic neuron projecting to the OB. We traced six cholinergic axons, and Figure 3 exhibits the representative data. We identified two types of projection patterns from the nuclei of origin to the OB. In one pattern, the axon

projected from HDB/MCPO, ascended through the medial septum, turned within the lateral septal nucleus, entered the dorsal tenia tecta, and finally reached the OB (Fig. 3A-D, axon colored in green). The axonal branches terminated in the lateral septal nucleus and anterior olfactory nucleus (AON, Fig. 3D). In the other type of projection pattern, the axon passed through the upper part of the olfactory tubercle, entered the ventral tenia tecta, and finally arrived at the OB (Fig. 3A-C and F, axon colored in blue). In the OB, the axon ramified and was distributed to several parts of the GL on both the ventral and dorsal sides (Fig. 3F). The cholinergic axon threaded its way through the periglomerular region around multiple glomeruli in the GL. The axon running through the periglomerular area had some branches which entered into glomeruli (Fig. 3G). Also, one of the traced axons which ramified in the GCL returned to the AON (Fig. 3A-C and E, axon colored in red). The summary of representative tracing data is exhibited in Table 2. The GL had the most branching and terminal endpoints of traced axons. Thus, the neuron tracing analysis in the present study revealed, for the first time, the complete projection pattern of a single cholinergic neuron.

Synaptic formation of cholinergic neurons in the OB

Recent findings of our EM study showed that serotonergic neurons form asymmetrical synapses with various thicknesses of PSD (Suzuki et al. 2015). To comparing with this serotonergic neuron data, we have performed morphometry measurements of the synapses of cholinergic neurons by electron microscopy tomography. Cholinergic fibers had varicosities similar to those of the serotonergic fibers. Figure 4A exhibits the tracing of an axon of the cholinergic neuron with varicosities. There were statistical differences in the number of varicosities per $50 \times 50 \times 10$ μm^3 among the layers (134 ± 11.85 in the

GL, 58 ± 9.87 in the EPL, 117 ± 16.29 in the IPL, 52 ± 5.35 in the GCL: GL vs. EPL or GCL; $p < 0.01$, IPL vs. EPL or GCL; $p < 0.01$, GL vs. IPL; $p = 0.088$, Fig. 4B). There were no statistical differences between the GL and the EPL regarding the number of varicosities per 10 μm of the axon (2.27 ± 0.35 in the GL, 2.25 ± 0.55 in the EPL; $p = 0.95$, Fig. 4C). Figure 4D-F exhibits representative synapses of the cholinergic neuron, serotonergic neuron, and olfactory receptor neuron, respectively. The preterminal and terminal parts of the ONs are characteristically electron-dense, and those terminals make typical synaptic contacts of the asymmetrical type (Pinching and Powell, 1971). VAChT-ir axons made asymmetrical synapses, having a clear active zone and medium-sized to large round vesicles. Dense-cored synaptic vesicles observed in the serotonergic neuron in our previous study (Suzuki et al., 2015) were not detected in the cholinergic neurons in this study. Synapses of the cholinergic neurons showed various PSD thicknesses (Fig. 4D). We confirmed that all of the synapses identified were formed with the varicose portion of the cholinergic axon. Cholinergic and serotonergic postsynaptic densities showed morphological differences compared to olfactory receptor neurons (Fig. 4D-F). To demonstrate distinctive features of these synapses, we examined synaptic components by EM tomography. These components, including the minor axis diameter of the synaptic vesicle, synaptic cleft size, and thickness of PSD, were measured to compare the values from the cholinergic or serotonergic neurons with those from the ONs (Fig. 4G). There was no statistically significant difference in the synaptic vesicle or synaptic cleft size between any neuron. However, in a comparison of PSD thickness, both cholinergic and serotonergic neurons differed from ONs in the measured values (Cholinergic; 24.3 ± 3.75 nm, Serotonergic; 26.28 ± 5.29 nm, ON; 33.6 ± 1.72 nm). The standard deviation of serotonergic neuron PSD thickness was significantly greater than

that of ON PSD thickness ($F = 9.398$, $p = 0.025$, Z-test). Additionally, the thickness of PSD of both cholinergic and serotonergic neurons showed significantly thinner values than ON PSD thickness (Cholinergic vs. ON; $p < 0.01$, Serotonergic vs. ON; $p < 0.05$, Cholinergic vs. Serotonergic; $p = 0.521$). These results indicate that synapses formed by cholinergic and serotonergic neurons in the GL have thinner PSDs as compared to typical asymmetrical synapses formed by ON.

To identify whether cholinergic neurons contain other neurotransmitters and to better understand how the cholinergic neuron acts on its target in the OB, we performed multiple immunostainings. Results from the CLSM study did not demonstrate obvious localization of VGLUT3 in the cholinergic axons of the OB (Fig. 5A). Also, no obvious VGAT immunoreactivity was observed in cholinergic axons (Fig. 5B). Our CLSM study demonstrated the expression of m2R in the majority of TH- ositive neurons. VAChT-ir varicosities were found in contiguity with the somata and dendrites of TH- positive neurons co-expressing m2R, suggesting synaptic formation. However, many somata and dendrites of TH- ositive neurons having no contact with cholinergic axonal varicosities also co-expressed m2R (Fig. 5C).

DISCUSSION

Using single-neuron tracing, we have revealed the complete projection pathway of the cholinergic axons from the HDB/MCPO to the OB, in particular detailed axonal tracts in the OB. Their axons were ramified and distributed to the AON. In the OB, axonal fibers innervated multiple olfactory glomeruli in different areas of the OB. A three-dimensional study with electron tomography demonstrated that cholinergic axons formed asymmetrical synapses with morphological variety in the GL. In addition, our results suggest extrasynaptic transmission in the OB, which has not been previously reported. The elucidation of axonal morphology provides an indispensable basis for the functional understanding of the neural circuit.

Methodological considerations

Cholinergic fibers immunolabeled for VAChT were thin, had small varicosities, and exhibited tortuous ramifications with multiple branches within the OB. Therefore, for more accurate visualization of projection pathways, we used ChAT-Cre mice and AAV vectors newly developed to express GFP in cholinergic neurons selectively. Furthermore, morphological characteristics of the cholinergic neurons labeled with AAV vectors resembled their structural features previously shown with immunocytochemistry. The numbers of neurons labeled with the viral vector method fluctuated in each injection experiments. We adjusted the viral titers and injection volumes to optimize the number of transfected neurons, approximately 30-40 neurons. We exhibited representative labeled neurons, which we could detect projection pathways through either anterograde tracing from the HDB/MCPO or retrograde tracing from the OB. This study demonstrated the

existence of at least two distinctive projection pathways. Although there were some variations, the majority of neurons appeared to be within these projection pathways based on our analysis.

The HVEM enables three-dimensional structure analysis with accurate morphometry. Furthermore, it can perform the analysis for the broad area up to a few dozen μm^2 with high resolution of less than 0.1 μm. Thus, these advantages cover both limitations of the resolution of CLSM and the evaluation area of EM. HVEM allows assessment of axonal morphology including varicosities that suggest synapse formation in the axon.

We have also performed a detailed morphological analysis of cholinergic neuron synaptic components using electron tomography. These elements have recently been used for synapse morphological analysis in other types of neurons (Burette et al., 2012; Perkins et al., 2015; Suzuki et al., 2015). In general, transmission electron microscope (TEM) extracts a two-dimensional projection image from an ultrathin section of 70 to 80 μm, preventing the detailed vertical information in the section. Microstructures are buried in the thick section with usual transmission images, and it is hard to perform detailed analysis such as synaptic component analysis. Electron tomography can provide a continuous sequence of tilted images, enabling a reconstruction transformed from a two-dimensional projection to a three-dimensional image which includes vertical information in the section (Frank, 1992, Perkins et al., 2015).

Cholinergic regulation of OB function

Some evidence has shown that the targets of cholinergic neurons in the OB are primarily localized in the GL and IPL based on axonal distribution density (Carson and

Burd, 1980; Le Jeune and Jourdan, 1993; Crespo et al., 1999; Salcedo et al., 2011). In this study, using wild-type mice, a high density of fibers immunoreactive for VAChT were also observed in the GL and IPL. We have examined the volume density of varicosities in the GL and IPL. However, since the number of varicosities per length of axon was the same in each layer, the number of branches in each layer and existence of terminals might influence the density. Cholinergic fibers labeled with AAV vector showed more branches in the GL than in other layers and ran randomly to cross multiple glomeruli with high-density innervation. Thus, this suggests that the GL is the area of primary activity for the cholinergic neurons in the OB.

Several electrophysiological studies have demonstrated that cholinergic activation causes excitation of mitral cells (Castillo et al., 1999; D'Souza and Vijayaraghavan, 2012; Zhan et al., 2013). However, different effects have been proposed in these studies using the current optogenetic methods. Stimulation of cholinergic neurons in the HDB inhibited spontaneous MTC spiking (Ma and Luo, 2012). On the other hand, stimulation of cholinergic axons in the OB increased MTC excitability (Rothermel et al., 2014). Furthermore, Rothermel et al. (2014) mentioned that HDB stimulation evoked a temporally complex modulation consisting of a brief initial excitation followed by a modest suppression of MTC spiking. It has been reported that cholinergic neurons project from the HDB/MCPO to the AON (Záborszky et al., 2012, Rothermel et al., 2015). It has also been reported that several types of neurons project from the AON to the OB (Soria-Gómez et al., 2014, Kay et al. 2014). The present study revealed that the same axon projecting to the OB has branches distributed into the AON. The evidence suggests that the cholinergic neurons projecting from the HDB/MCPO have multiple actions in the OB: direct innervation, and indirect action via axonal branches in

the AON. The branching patterns of cholinergic axons seen in this study could help explain such different functional results.

Neural oscillations associated with learning and memory formation (Igarashi et al., 2014) have been observed even in the OB and the olfactory cortical area such as piriform cortex (Ravel et al., 2003). Cholinergic modulation is associated with the generation of this oscillation (Lawrence, 2008, Tsuno et al., 2008). Furthermore, the computational model from diverse physiological studies has suggested that cholinergic activity serves to increase lateral inhibition and sharpen the odor receptive field of MTCs (Linster and Cleland, 2002). Axonal branches in the OB were also distributed disorderly throughout all layers and crossed into multiple adjacent glomeruli in the GL. Because of their widespread targets, the intricate branching patterns could influence control of neural activities and functions, including odor identification and discrimination.

Synaptic formation

Some reports have demonstrated the synaptic formation of cholinergic axons on dendrites and somata of periglomerular (PG) cells and short axon cells in the GL of the rat OB (Le Juene and Jourdan, 1993; Kasa et al., 1995). Furthermore, cholinergic axons have been shown to make synapses on type 1 and type 2 PG cells in the GL of the cynomolgus monkey OB (Liberia et al., 2015). Representative type 1 PG cells, containing TH and nitric oxide synthase (NOS), are GABA-ir and are innervated by ONs. Type 2 PG cells, containing calretinin and calbindin, are GABA-ir and are less innervated by ONs (Kosaka et al., 1997; Kosaka and Kosaka, 2005). Type 1 and Type 2 PG cells are mainly associated with regulating various olfactory functions such as odor discrimination and recognition, respectively (Toida, 2008). The synapses of the cholinergic axons in the OB

have previously been classified as asymmetrical synapses (Kasa et al., 1995). However, Liberia et al. (2015) were uncertain in determining a symmetrical or an asymmetrical classification, because synaptic contacts had an "ambiguous" postsynaptic thickening and presynaptic boutons contained numerous medium-sized to large round vesicles. Suzuki et al. (2015) have revealed a variety of PSD thicknesses in morphological analysis of the synapses for serotonergic axons in the GL of the OB. Serotonergic neurons projecting toward the OB also contain glutamic acid as a neurotransmitter and have multiple receptors in the postsynaptic element. Therefore, various stimulation patterns could be one of the reasons for such variety at the PSD. A previous study showed that cholinergic neurons also express VGLUT3 in the striatum (Gras et al., 2002). Co-expression with GABA has been identified in cholinergic amacrine cells in the retina (Nguyen et al., 2000). The cholinergic axons in the OB might also have several other neurotransmitters. However, we have not yet identified other transmitters in the cholinergic neurons projecting to the OB with the limits of our current method. This study demonstrated that the cholinergic axons, like the serotonergic axons, show different types of PSD, unlike olfactory receptor neurons which only form typical asymmetrical synapses. It has been suggested that scaffold proteins are integral to forming the PSD (Petersen et al., 2003), and previous studies have shown that several scaffold proteins co-localize at cholinergic synapses of autonomic ganglia in mice (Brenman et al., 1996, Krishnaswamy and Cooper, 2009). Furthermore, it has been reported that scaffold proteins bind to cholinergic receptors (Hoshi et al., 2005). Therefore, we suggest that there might be subtypes of cholinergic receptors and numerous scaffold proteins contributing to variety in synaptic morphology.

Cholinergic transmission

In the adult rat central nervous system, it has been reported that the value of synaptic incidence for cholinergic axon boutons synapsing with the dendritic trunk and dendritic spines is 14% in the cerebral cortex (Par1), 7% in the hippocampus (CA1) (Umbriaco et al., 1994, 1995), and 9% in the neostriatum (Contant et al., 1996). In the OB, the percent of cholinergic axon varicosities below the GL was about 2% (Kasa et al., 1995). Although there were statistical differences in the density of varicosities among layers, no statistical differences in the number of varicosities per cholinergic fiber have been observed in the different layers. This result indicates that the number of synapses was greater in the GL and the IPL compared to the other OB layers.

Previous studies that have analyzed the ratio of cholinergic pre- to postsynaptic structures quantitatively have strongly supported volume transmission of acetylcholine (Mrzljak et al., 1993; Descarries et al., 1997). In this mode, cholinergic neurotransmission is capable of escaping the synapse to stimulate distant, extrasynaptic acetylcholine (ACh) receptors (Agnati et al., 2006). ACh is released at extrasynaptic sites despite the absence of postsynaptic targets in the immediate area, resulting in long-latency and prolonged effects (Descarries et al., 1997; Sarter et al., 2009). Cholinergic activities of the PG cells also vary depending on receptor type (Castillo et al., 1999; Pignatelli and Belluzzi, 2008; Ma and Luo, 2012). Crespo et al. (2000) demonstrated that TH neurons are a subset of PG cells which express m2R. Electrophysiological studies have shown that activation of m2R by acetylcholine inhibits dopaminergic PG cells (Pignatelli and Belluzzi, 2008). In the previous EM study, the extrasynaptic plasma membrane of the dendrite is possibly the primary site for m2R activation, considering the previously-demonstrated neuron surface distribution of m2R in dendrite in other brain regions (Mrzljak et al., 1993, Bernard et al.,

1998). Predominant distribution of immunogold particles recognizing m2R in the extrasynaptic plasma membrane of dendrite in addition to its cytosol (Garzón and Pickel, 2016) is consistent with m2R activation by extrasynaptic diffusion of ACh (Umbriaco et al., 1994). In the present study, we have also shown the expression of m2R in the majority of TH-ir neurons in the GL, but many somata and dendrites of those with no contact with VAChT-ir varicosities also expressed m2R. It has been suggested that ACh, which is released at extrasynaptic sites, acts on these receptors. This result lends anatomical support of volume transmission of ACh in the OB.

Future studies

Approximately 15% of the neurons projecting from the HDB/MCPO to OB are cholinergic (data not shown), which is consistent with the previous report about the rat OB (Záborszky et al. 1986). The HDB/MCPO also contains GABAergic neurons projecting to the OB (Záborszky et al. 1986, Gracia-Llanes et al., 2010). The majority of the cholinergic projection neurons are located in the medial half of the HDB/MCPO. In contrast, the GABAergic projection neurons primarily lie in the caudal part of the HDB/MCPO, especially in its lateral part (Záborszky et al. 1986). These results indicate the difference of cellular location by neuron types in the nuclei of origin. In this study, we have elucidated that there were at least two projection patterns from HDB/MCPO to the OB in the cholinergic neurons. Further analysis would be necessary to evaluate if each projection pathway and distribution of axon terminals in the OB are attributed to unique locations of various neuron cell types such as GABAergic and cholinergic neurons.

CONCLUSION

We have successfully elucidated the overall morphological characterization of the cholinergic neurons projecting from HDB/MCPO to the OB (Fig. 6). The same single cholinergic axon branched into multiple different areas in the glomerular layer of the OB, and these branches innervated multiple glomeruli. We confirmed a variety of PSD thicknesses of cholinergic axons using electron tomography. Furthermore, our results indicate that cholinergic neurons utilize dual types of transmission in the OB. Thus, this evidence suggests that acetylcholine contributes to the modulation of olfactory neural circuits in a sophisticated manner. We plan to focus on the analysis of synaptic targets, including receptors, as our next step.

ACKNOWLEDGMENT

We thanks Prof. Takeshi Kaneko and Dr. Takahiro Furuta of Kyoto University for providing adeno-associated viral vectors, Ms. Rie Ohmori of the Department of Anatomy, Mr. Nobuyuki Matsuda, Ms. Kazuko Yamane of the Central Research Institute of Kawasaki Medical school for their technical assistance, Dr. Renee E. Cockerham of the Program in Neuroscience, the University of Maryland School of Medicine for valuable comments and proofreading of this article; and Dr. Kazuyoshi Murata and Dr. Tatsuo Arii of the National Institute for Physiological Sciences at Okazaki, Japan, for assistance with the high voltage electron microscopy (H-1250M). This work was supported by MEXT/JSPS KAKENHI Grant Numbers JP15K06748, JP24500418, JP23500419, JP24500408, JP15K14333, JP25123709, JP15H01430, JP16H01426, JP16H04663.

CONFLICT OF INTEREST

No author has any conflict of interest.

ROLE OF AUTHORS

All authors had full access to all the data in the study and take responsibility for the integrity of the data and the accuracy of the data analysis. Study concept and design: Kazunori Toida. Acquisition of data: Masakazu Hamamoto. Analysis and interpretation of data: Masakazu Hamamoto, Emi Kiyokage, and Kazunori Toida. Drafting of the manuscript: Masakazu Hamamoto. Critical revision of the manuscript for important intellectual content: Emi Kiyokage and Kazunori Toida. Statistical analysis: Masakazu Hamamoto. Obtained funding: Masakazu Hamamoto, Emi Kiyokage, Jaerin Sohn, Hiroyuki Hioki, and Kazunori Toida. Administrative, technical, and material support: Emi Kiyokage, Jaerin Sohn, Hiroyuki Hioki, and Kazunori Toida. Production of virus vector: Jaerin Sohn and Hiroyuki Hioki. Study supervision: Kazunori Toida.

LITERATURE CITED

Agnati LF, Leo G, Zanardi A, Genedani S, Rivera A, Fuxe K, Guidolin D. 2006. Volume transmission and wiring transmission from cellular to molecular networks: history and perspectives. Acta Physiol (Oxf) 187: 329-344.

Bernard V, Laribi O, Levey AI, Bloch B. 1998. Subcellular redistribution of m2 muscarinic acetylcholine receptors in striatal interneurons in vivo after acute cholinergic stimulation. J Neurosci 18: 10207-10218.

Burette AC, Lesperance T, Crum J, Martone M, Volkmann N, Ellisman MH, Weinberg RJ. 2012. Electron tomographic analysis of synaptic ultrastructure. J Comp Neurol 520: 2697-2711.

Bregman BS. 1987. Development of serotonin immunoreactivity in the rat spinal cord and its plasticity after neonatal spinal cord lesions. Brain Res 431:245–263.

Brenman JE, Christopherson KS, Craven SE, McGee AW, Bredt DS. 1996. Cloning and characterization of postsynaptic density 93, a nitric oxide synthase interacting protein. J Neurosci 16: 7407-7415.

Carson KA. 1984a. Quantitative localization of neurons projecting to the mouse main olfactory bulb. Brain Res Bull 12: 629-634.

Carson KA. 1984b. Localization of acetylcholinesterase-positive neurons projecting to the mouse main olfactory bulb. Brain Res Bull 12: 635-639.

Carson KA, Burd GD. 1980. Localization of acetylcholinesterase in the main and accessory olfactory bulbs of the mouse by light and electron microscopic histochemistry. J Comp Neurol 191: 353-371.

Castillo PE, Carleton A, Vincent JD, Lledo PM. 1999. Multiple and opposing roles of cholinergic transmission in the main olfactory bulb. J Neurosci 19: 9180-9191.

Collier TJ, Sortwell CE, Daley BF. 1999. Diminished viability, growth, and behavioral efficacy of fetal dopamine neuron grafts in aging rats with long-term dopamine depletion: an argument for neurotrophic supplementation. J Neurosci 19: 5563-5573.

Contant C, Umbriaco D, Garcia S, Watkins KC, Descarries L. 1996. Ultrastructural characterization of the acetylcholine innervation in adult rat neostriatum. Neuroscience 71: 937-947.

Crespo C, Blasco-Ibáñez JM, Briñón JG, Alonso JR, Domínguez MI, Martínez-Guijarro FJ. 2000. Subcellular localization of m2 muscarinic receptors in GABAergic interneurons of the olfactory bulb. Eur J Neurosci 12: 3963-3974.

Crespo C, Briñón JG, Porteros A, Arévalo R, Rico B, Aijón J, Alonso JR. 1999. Distribution of acetylcholinesterase and choline acetyltransferase in the main and accessory olfactory bulbs of the hedgehog (Erinaceus europaeus). J Comp Neurol 403: 53-67.

D'Souza RD, Vijayaraghavan S. 2012. Nicotinic receptor-mediated filtering of mitral cell responses to olfactory nerve inputs involves the α3β4 subtype. J Neurosci 32: 3261-3266.

Descarries L, Gisiger V, Steriade M. 1997. Diffuse transmission by acetylcholine in the CNS. Prog Neurobiol 53: 603-625.

Elaagouby A, Ravel N, Gervais R. 1991. Cholinergic modulation of excitability in the rat olfactory bulb: effect of local application of cholinergic agents on evoked field potentials. Neuroscience 45: 653-662.

Escanilla O, Alperin S, Youssef M, Ennis M, Linster C. 2012. Noradrenergic but not cholinergic modulation of olfactory bulb during processing of near threshold concentration stimuli. Behav Neurosci 126: 720)'28.

Fletcher ML, Chen WR. 2010. Neural correlates of olfactory learning: Critical role of centrifugal neuromodulation. Learn Mem 17:561-570.

Frank J. 1992. Electron tomography: Three dimensional imaging with the transmission electron microscope. New York. Plenum Press.

Fremeau RT, Burman J, Qureshi T, Tran CH, Proctor J, Johnson J, Zhang H, Sulzer D, Copenhagen DR, Storm-Mathisen J, Reimer RJ, Chaudhry FA, Edwards RH. 2002. The identification of vesicular glutamate transporter 3 suggests novel modes of signaling by glutamate. Proc Natl Acad Sci USA 99: 14488-14493.

Garzón M, Pickel VM. 2016. Electron Microscopic Localization of M2-muscarinic receptors in Cholinergic and Non-Cholinergic Neurons of the Laterodorsal Tegmental and Pedunculopontine Nuclei of the Rat Mesopontine Tegmentum. J Comp Neurol 524:3084-3103.

Gilmor ML, Nash NR, Roghani A, Edwards RH, Yi H, Hersch SM, Levey AI. 1996. Expression of the putative vesicular acetylcholine transporter in rat brain and localization in cholinergic synaptic vesicles. J Neurosci 16: 2179-2190.

Gracia-Llanes FJ, Crespo C, Blasco-Ibáñez JM, Nacher J, Varea E, Rovira-Esteban L, Martínez-Guijarro FJ. 2010. GABAergic basal forebrain afferents innervate selectively GABAergic targets in the main olfactory bulb. Neuroscience 170: 913-922.

Gras C, Herzog E, Bellenchi GC, Bernard V, Ravassard P, Pohl M, Gasnier B, Giros B, El Mestikawy S. 2002. A third vesicular glutamate transporter expressed by cholinergic and serotoninergic neurons. J Neurosci 22: 5442-5451.

Guo C, Stella SL, Hirano AA, Brecha NC. 2009. Plasmalemmal and vesicular gamma-aminobutyric acid transporter expression in the developing mouse retina. J Comp Neurol 512: 6-26.

Hassani OK, Lee MG, Henny P, Jones BE. 2009. Discharge profiles of identified GABAergic in comparison to cholinergic and putative glutamatergic basal forebrain neurons across the sleep-wake cycle. J Neurosci 29: 11828-11840.

Hasselmo ME. 1999. Neuromodulation: acetylcholine and memory consolidation. Trends Cogn Sci 3: 351-359.

Hioki H, Nakamura H, Ma YF, Konno M, Hayakawa T, Nakamura KC, Fujiyama F, Kaneko T. 2010. Vesicular glutamate transporter 3-expressing nonserotonergic

projection neurons constitute a subregion in the rat midbrain raphe nuclei. J Comp Neurol 518: 668-686.

Hoshi N, Langeberg LK, Scott JD. 2005. Distinct enzyme combinations in AKAP signalling complexes permit functional diversity. Nat Cell Biol 7: 1066-1073.

Ichikawa T, Ajiki K, Matsuura J, Misawa H. 1997. Localization of two cholinergic markers, choline acetyltransferase and vesicular acetylcholine transporter in the central nervous system of the rat: in situ hybridization histochemistry and immunohistochemistry. J Chem Neuroanat 13: 23-39.

Igarashi KM, Lu L, Colgin LL, Moser MB, Moser EI. 2014. Coordination of entorhinal-hippocampal ensemble activity during associative learning. Nature 510: 143-147.

Jositsch G, Papadakis T, Haberberger RV, Wolff M, Wess J, Kummer W. 2009. Suitability of muscarinic acetylcholine receptor antibodies for immunohistochemistry evaluated on tissue sections of receptor gene-deficient mice. Naunyn Schmiedebergs Arch Pharmacol 379:389–395.

Kasa P, Hlavati I, Dobo E, Wolff A, Joo F, Wolff JR. 1995. Synaptic and non-synaptic cholinergic innervation of the various types of neurons in the main olfactory bulb of adult rat: immunocytochemistry of choline acetyltranceferase. Neuroscience 67: 667-677.

Kay RB, Brunjes PC. 2014. Diversity among principal and GABAergic neurons of the anterior olfactory nucleus. Front Cell Neurosci 8:111.

1 Kosaka K, Kosaka T. 2005. Synaptic organization of the glomerulus in the main
2 olfactory bulb: compartments of the glomerulus and heterogeneity of the
3 periglomerular cells. Anat Sci Int 80: 80-90.

4 Kosaka K, Toida K, Margolis FL, Kosaka T. 1997. Chemically defined neuron groups
5 and their subpopulations in the glomerular layer of the rat main olfactory
6 bulb--II. Prominent differences in the intraglomerular dendritic arborization and
7 their relationship to olfactory nerve terminals. Neuroscience 76: 775-786.

8 Krishnaswamy A, Cooper E. 2009. An activity-dependent retrograde signal induces the
9 expression of the high-affinity choline transporter in cholinergic neurons.
10 Neuron 61: 272-286.

11 Lawrence JJ. 2008. Cholinergic control of GABA release: emerging parallels between
12 neocortex and hippocampus. Trends Neurosci 31: 317-327.

13 Lejeune H, Jourdan F. 1993. Cholinergic innervation of olfactory glomeruli in
14 the rat: an ultrastructural immunocytochemical study. Journal of Comparative
15 Neurology 336: 279-292.

16 Levey AI, Edmunds SM, Hersch SM, Wiley RG, Heilman CJ. 1995. Light and electron
17 microscopic study of m2 muscarinic acetylcholine receptor in the basal
18 forebrain of the rat. J Comp Neurol 351:339–356.

19 Liberia T, Blasco-Ibáñez JM, Nácher J, Varea E, Lanciego JL, Crespo C. 2015. Synaptic
20 connectivity of the cholinergic axons in the olfactory bulb of the cynomolgus
21 monkey. Front Neuroanat 9:28.

Linster C, Cleland TA. 2002. Cholinergic modulation of sensory representations in the olfactory bulb. Neural Netw 15: 709-717.

Ma M, Luo M. 2012. Optogenetic Activation of Basal Forebrain Cholinergic Neurons Modulates Neuronal Excitability and Sensory Responses in the Main Olfactory Bulb. Journal of Neuroscience 32: 10105-10116.

Macrides F, Davis BJ, Youngs WM, Nadi NS, Margolis FL. 1981. Cholinergic and catecholaminergic afferents to the olfactory bulb in the hamster: a neuroanatomical, biochemical, and histochemical investigation. J Comp Neurol 203: 495-514.

Mandairon N, Ferretti CJ, Stack CM, Rubin DB, Cleland TA, Linster C. 2006. Cholinergic modulation in the olfactory bulb influences spontaneous olfactory discrimination in adult rats. Eur J Neurosci 24: 3234-3244.

McLean JH, Shipley MT. 1987. Serotonergic afferents to the rat olfactory bulb: I. Origins and laminar specificity of serotonergic inputs in the adult rat. J Neurosci 7: 3016-3028.

Micheva KD, Busse B, Weiler NC, O'Rourke N, Smith SJ. 2010. Single-synapse analysis of a diverse synapse population: proteomic imaging methods and markers. Neuron 68: 639-653.

Mrzljak L, Levey AI, Goldman-Rakic PS. 1993. Association of m1 and m2 muscarinic receptor proteins with asymmetric synapses in the primate cerebral cortex:

morphological evidence for cholinergic modulation of excitatory neurotransmission. Proc Natl Acad Sci USA 90: 5194-5198.

Nguyen LT, Grzywacz NM. 2000. Colocalization of choline acetyltransferase and gamma-aminobutyric acid in the developing and adult turtle retinas. J Comp Neurol 420: 527-538.

Nickell WT, Shipley MT. 1988. Neurophysiology of magnocellular forebrain inputs to the olfactory bulb in the rat: frequency potentiation of field potentials and inhibition of output neurons. J Neurosci 8:4492-4502.

Perkins GA, Jackson DR, Spirou GA. 2015. Resolving presynaptic structure by electron tomography. Synapse 69: 268-282.

Petersen JD, Chen X, Vinade L, Dosemeci A, Lisman JE, Reese TS. 2003. Distribution of postsynaptic density (PSD)-95 and Ca2+/calmodulin-dependent protein kinase II at the PSD. J Neurosci 23: 11270-11278.

Pignatelli A, Belluzzi O. 2008. Cholinergic modulation of dopaminergic neurons in the mouse olfactory bulb. Chem Senses 33: 331-338.

Pinching AJ, Powell TP. 1971. The neuropil of the glomeruli of the olfactory bulb. J Cell Sci 9: 347-377.

Ravel N, Chabaud P, Martin C, Gaveau V, Hugues E, Tallon-Baudry C, Bertrand O, Gervais R. 2003. Olfactory learning modifies the expression of odour-induced oscillatory responses in the gamma (60-90 Hz) and beta (15-40 Hz) bands in the rat olfactory bulb. Eur J Neurosci 17: 350-358.

Rothermel M, Carey RM, Puche A, Shipley MT, Wachowiak M. 2014. Cholinergic inputs from Basal forebrain add an excitatory bias to odor coding in the olfactory bulb. J Neurosci 34: 4654-4664.

Salcedo E, Tuan T, Ly X, Lopez R, Barbica C, Restrepo D, Vijayaraghavan S. 2011. Activity-Dependent Changes in Cholinergic Innervation of the Mouse Olfactory Bulb. Plos One 6.

Sarter M, Parikh V, Howe WM. 2009. Phasic acetylcholine release and the volume transmission hypothesis: time to move on. Nat Rev Neurosci 10: 383-390.

Shepherd GM., Chen W.R. and Greer C.A. 2004. Olfactory bulb. In Shepherd G.M. (Ed.), *The Synaptic organization of the brain.* Edn 5. New York. Oxford University Press: 165-216.

Shipley MT, Halloran FJ, de la Torre J. 1985. Surprisingly rich projection from locus coeruleus to the olfactory bulb in the rat. Brain Res 329: 294-299.

Soria-Gómez E, Bellocchio L, Reguero L, Lepousez G, Martin C, Bendahmane M, Ruehle S, Remmers F, Desprez T, Matias I, Wiesner T, Cannich A, Nissant A, Wadleigh A, Pape HC, Chiarlone AP, Quarta C, Verrier D, Vincent P, Massa F, Lutz B, Guzmán M, Gurden H, Ferreira G, Lledo PM, Grandes P, Marsicano G. 2014. The endocannabinoid system controls food intake via olfactory processes. Nat Neurosci 17: 407-415.

Suzuki Y, Kiyokage E, Sohn J, Hioki H, Toida K. 2015. Structural basis for serotonergic regulation of neural circuits in the mouse olfactory bulb. J Comp Neurol 523: 262-280.

Takamori S, Riedel D, Jahn R. 2000. Immunoisolation of GABA-specific synaptic vesicles defines a functionally distinct subset of synaptic vesicles. J Neurosci 20: 4904-4911.

Takashima Y, Daniels RL, Knowlton W, Teng J, Liman ER, McKemy DD. 2007. Diversity in the neural circuitry of cold sensing revealed by genetic axonal labeling of transient receptor potential melastatin 8 neurons. J Neurosci 27: 14147-14157.

Tatti R, Bhaukaurally K, Gschwend O, Seal RP, Edwards RH, Rodriguez I, Carleton A. 2014. A population of glomerular glutamatergic neurons controls sensory information transfer in the mouse olfactory bulb. Nat Commun 5:3791.

Toida K, Kosaka K, Aika Y, Kosaka T. 2000. Chemically defined neuron groups and their subpopulations in the glomerular layer of the rat main olfactory bulb--IV. Intraglomerular synapses of tyrosine hydroxylase-immunoreactive neurons. Neuroscience 101: 11-17.

Toida K. 2008. Synaptic organization of the olfactory bulb based on chemical cording of neurons. Anat Sci Int 83: 207-217.

Toida K., Kosaka K., Aika Y., Kosaka T. 2002. Cathecolaminergic neurons in the olfactory bulb. In Nagatsu T., Nabeshima R., McCarthy R., Goldstein D (Eds.),

Cathecholamine Research: From Molecular Insights to Clinical Medicine. Kluwer, New York: 289-292.

Toida K, Kosaka K, Heizmann CW, Kosaka T. 1998. Chemically defined neuron groups and their subpopulations in the glomerular layer of the rat main olfactory bulb: III. Structural features of calbindin D28K-immunoreactive neurons. J Comp Neurol 392: 179-198.

Tsuno Y, Kashiwadani H, Mori K. 2008. Behavioral state regulation of dendrodendritic synaptic inhibition in the olfactory bulb. J Neurosci 28: 9227-9238.

Tsutsumi T, Houtani T, Toida K, Kase M, Yamashita T, Ishimura K, Sugimoto T. 2007. Vesicular acetylcholine transporter-immunoreactive axon terminals enriched in the pontine nuclei of the mouse. Neuroscience 146: 1869-1878.

Umbriaco D, Garcia S, Beaulieu C, Descarries L. 1995. Relational features of acetylcholine, noradrenaline, serotonin and GABA axon terminals in the stratum radiatum of adult rat hippocampus (CA1). Hippocampus 5: 605-620.

Umbriaco D, Watkins KC, Descarries L, Cozzari C, Hartman BK. 1994. Ultrastructural and morphometric features of the acetylcholine innervation in adult rat parietal cortex: an electron microscopic study in serial sections. J Comp Neurol 348: 351-373.

Wenk GL. 1997. The nucleus basalis magnocellularis cholinergic system: one hundred years of progress. Neurobiol Learn Mem 67: 85-95.

Woolf NJ, Eckenstein F, Butcher LL. 1984. Cholinergic systems in the rat brain: I. projections to the limbic telencephalon. Brain Res Bull 13: 751-784.

Zhan X, Yin P, Heinbockel T. 2013. The basal forebrain modulates spontaneous activity of principal cells in the main olfactory bulb of anesthetized mice. Front Neural Circuits 7:148.

Záborszky L, Carlsen J, Brashear HR, Heimer L. 1986. Cholinergic and GABAergic afferents to the olfactory bulb in the rat with special emphasis on the projection neurons in the nucleus of the horizontal limb of the diagonal band. J Comp Neurol 243: 488-509.

Záborszky L, Van Den Pol AN, and Gyengesi E. 2012. The basal forebrain cholinergic projection system in mice. In Watson C, Paxinos G and Puelles L (Eds.), The Mouse Nervous System. Amsterdam. Elsevier: 684–718.

Figure 1. Immunocytochemistry of cholinergic neurons with the anti-VAChT antibody. (**A**) Cholinergic neurons widely distributed in various brain regions. (**B**) VAChT-ir somata were found in the HDB/MCPO. (**C**) Co-expression of ChAT and VAChT in the HDB/MCPO. **C1** shows ChAT-ir (green), **C2** shows VAChT-ir (magenta), **C3** shows the double overlay. (**D**) Cholinergic fibers were distributed densely in the glomerular layer (GL) and internal plexiform layer (IPL). (**E**) Light microscopy image for observation of HVEM. (**F**) A stereo pair of HVEM (± 8°) images showing cholinergic axons in the glomerular and periglomerular regions with branches and varicosities. (**G**) Quantification of VAChT-ir fiber density was measured by the ROD ratio of each layer to EPL. The majority of fibers were found in the GL and IPL (* $p < 0.05$ and ** $p < 0.01$ compared with EPL). ChAT, choline acetyltransferase; EPL, external plexiform layer; GCL, granule cell layer; HDB, horizontal limb of the diagonal band of Broca; HVEM, high-voltage electron microscopy; -ir, immunoreactive; MCL, mitral cell layer; MCPO, magnocellular preoptic nucleus; ROD, relative optical density; ONL, olfactory nerve layer; VAChT, vesicular acetylcholine transporter. Scale bars = 2 mm in A; 200 μm in B; 50 μm in D; 25 μm in C and E; 10 μm in F.

Figure 2. Selective labeling of the cholinergic neuron by viral injection. (**A**) Double immunolabeling for characterization of cholinergic neurons in the HDB/MCPO. **A1** shows infected neurons (green), **A2** shows cholinergic neurons (magenta), and **A3** shows the double overlay. All infected neurons in the HDB/MCPO were cholinergic neurons. (**B**) Fluorescent labeling was converted to bright field labeling in the HDB/MCPO. (**C-F**) DAB visualization of infected axons in the olfactory bulb. (**C**) Infected cholinergic fibers were most densely distributed in the glomerular layer (GL).

(**D**) In the GL, the majority of fibers repeatedly branched and crossed into the adjacent glomeruli (arrowheads). (**E**) In the external plexiform layer (EPL), a small number of fibers which bifurcated were found ascending to the GL. (**F**) In the granule cell layer (GCL), multiple branching fibers were frequently found. GFP, green fluorescent protein; MCPO, magnocellular preoptic nucleus; HDB, horizontal limb of the diagonal band of Broca. Scale bars = 20μm in A; 100 μm in B and C; 50 μm in F.

Figure 3. Three-dimensional reconstructions of three cholinergic neurons from the HDB/MCPO to the olfactory bulb (OB). Each cholinergic neuron was reconstructed after infection of ChAT-Cre mice with AAV. (**A**) Lateral view. (**B**) Dorsal view. (**C**) Rostral view. (**D**) A single axon had branches to the lateral septum nucleus and anterior olfactory nucleus (AON). (**E**) An axon left the OB and returned to the AON. (**F**) In the OB, a single axon traveled with multiple ramifications and distributed in both ventral and dorsal sides of the glomerular layer (GL). (**G**) In the GL, an axon passed through the periglomerular region. Individual glomeruli in the GL are shown in different colors. AAV, adeno-associated virus; ChAT, choline acetyltransferase; HDB, horizontal limb of the diagonal band of Broca; MCPO, magnocellular preoptic nucleus. Scale bars = 2 mm in A (applies B and C); 1 mm in D and F (applies to E); 100 μm in G.

Figure 4. Morphometry of cholinergic neurons and synaptic features.
(**A,A1**)Reconstruction of a cholinergic axon. The axon ascended vertically from the granule cell layer (GCL) to the glomerular layer (GL). The axon bifurcated four times within the glomeruli, and one of the axonal branches entered into each of the neighboring glomeruli (Stereo pairs of 3D reconstruction images ± 8°). A red circle

indicates a varicosity. (**B**) The mean number of varicosities per 50 x 50 x 10 μm^3 in each layer. The majority of varicosities were found in the GL and IPL (*p < 0.01 compared with EPL or GCL, Student's t-test). (**C**) The mean number of varicosities per 10 μm in the GL and the external plexiform layer (EPL). There was no significant difference between the GL and EPL. Electron microscopic images of synapses in the GL (**D-F**, arrowheads). Synaptic terminals of cholinergic (**D**), serotonergic (**E**), and olfactory receptor neurons (**F**). Morphometry of synaptic vesicles, synaptic cleft, and thickness of PSD (**G**). There was no statistically significant difference in the synaptic vesicle or synaptic cleft size between the three neurons. There was a statistical difference between the variance of the thickness of PSD of 5-HT neurons and that of olfactory receptor neurons ($F = 9.39$, $p = 0.025$, Z-test). Moreover, there was a statistical difference between the mean of the thickness of the PSDs (Cholinergic vs. ONs; **p < 0.01, student's t-test, Serotonergic vs. ONs; *p < 0.05, Welch test). IPL, internal plexiform layer; MCL, mitral cell layer; ON, olfactory receptor neuron; PSD, postsynaptic density; 3D, three-dimensional; 5-HT, 5-hydroxytryptamine (serotonergic). Scale bars = 50 μm in A; 200 nm in D-F.

Figure 5. Localization of m2R in the glomerular layer (GL). Double immunostaining shows that VGLUT3 (**A**) and VGAT (**B**) were not co-localized in varicosities expressing VAChT. (**C**) Multiple immunostainings of m2R (green, **C1**), TH (green, **C2**), and VAChT (magenta, **C3**). Expression of m2R was found on TH-ir somata and processes, which are occasionally associated with VAChT-ir varicosities (arrowheads). Most of the m2R-ir puncta did not associate with VAChT-ir. -ir, immunoreactive; m2R, m2 muscarinic acetylcholine receptor; TH, tyrosine hydroxylase; VAChT, vesicular acetylcholine

transporter; VGAT, vesicular GABA transporter; VGLUT3, vesicular glutamate transporter 3. Scale bars = 20 μm in B (applies to A) and C.

Figure 6. Concluding scheme. Taken together with our previous findings, cholinergic neurons originating from HDB/MCPO project to the OB branching multiple times, distribute to glomeruli localized in different areas of the GL and influence bulbar interneurons.

ACh, acetylcholine; AON, anterior olfactory nucleus; EPL, external plexiform layer; GCL, granule cell layer; GL, glomerular layer; HDB, horizontal limb of the diagonal band of Broca; IPL, internal plexiform layer; MCL, mitral cell layer; MCPO, magnocellular preoptic nucleus; OB, olfactory bulb; TH, tyrosine hydroxylase. a (red), asymmetrical synapse; s (blue), symmetrical synapse.

Table 1. Table of Primary Antibodies Used

Antigen	Description of Immunogen	Source, Host Species, Cat#, Clone or Lot#, RRID	Working dilution
VAChT	Peptide at the N-terminus of human VAChT(aa 1-33)	Santa Cruz, Goat polyclonal, Cat# sc-7717, Lot# D0914, RRID: AB_2301794	1:500
ChAT	Human placental enzyme	Millipore, Rabbit polyclonal, Lot# 2065414, Cat#AB143 RRID: AB_2079760	1:5,000
GFP	GFP isolated directly from the jellyfish *Aequorea victoria*	Life Technology, Chicken polyclonal, Cat# A10262, Lot# 1229709, RRID: AB_11180610	1:10,000
VGAT	Synthetic peptide AEPPVEGDIHYQR (aa 75 - 87 in rat) coupled to key-hole limpet hemocyanin via an added N- terminal cysteine	Synaptic Systems, Mouse monoclonal, Cat# 131011, RRID: AB_1966444	1:5,000
VGLUT3	Recombinant C-terminus of mouse VGLUT 3 (aa 543 - 601).	Synaptic Systems, Rabbit polyclonal, Cat# 135203, RRID: AB_2187708	1:1,000

m2R	i3 loop of m2 receptor fusion protein (aa 225-359), fused to Glutathione S-transferase	Millipore, Rat monoclonal, Cat# MAB367, Lot# 2506486, RRID: AB_94952	1:1,000
Tyrosine Hydroxylase	Purified TH from PC12 cells	Millipore, Mouse monoclonal, Cat# AB318, Lot# 25040117, RRID: AB_2315522	1:5,000
5-HT	Serotonin coupled to bovine serum albumin	Immunostar, Rabbit polyclonal, Cat# 20080, Lot# 541317, RRID: AB_572263	1:50,000

Abbreviations: aa, amino acids; VAChT, vesicular acetylcholine transporter; ChAT, choline acetyltransferase; GFP, green fluorescent protein; VGAT, vesicular GABA transporter; VGLUT3, vesicular glutamate transporter 3; m2R, m2 muscarinic acetylcholine receptor; 5-HT, 5-hydroxytryptoamine

Table 2. Summary of tracing data for cholinergic axons from the HDB/MCPO to the OB (in Fig. 3)

	Total traced length (μm)	Number of branching point in the OB				Number of endpoint in the OB			
		GL	EPL	IPL	GCL	GL	EPL	IPL	GCL
#1 (colored in green)	16,529.9	-	-	-	7	-	-	-	9
#2 (colored in red)	15,941.8	-	-	-	9	-	-	-	9
#3 (colored in blue)	29,839.9	30	2	24	5	41	0	20	4

Abbreviations: HDB, horizontal limb of the diagonal band; MCPO, magnocellular preoptic nucleus; GL, glomerular layer; EPL, external plexiform layer; IPL, internal plexiform layer; GCL, granule cell layer; OB, olfactory bulb.

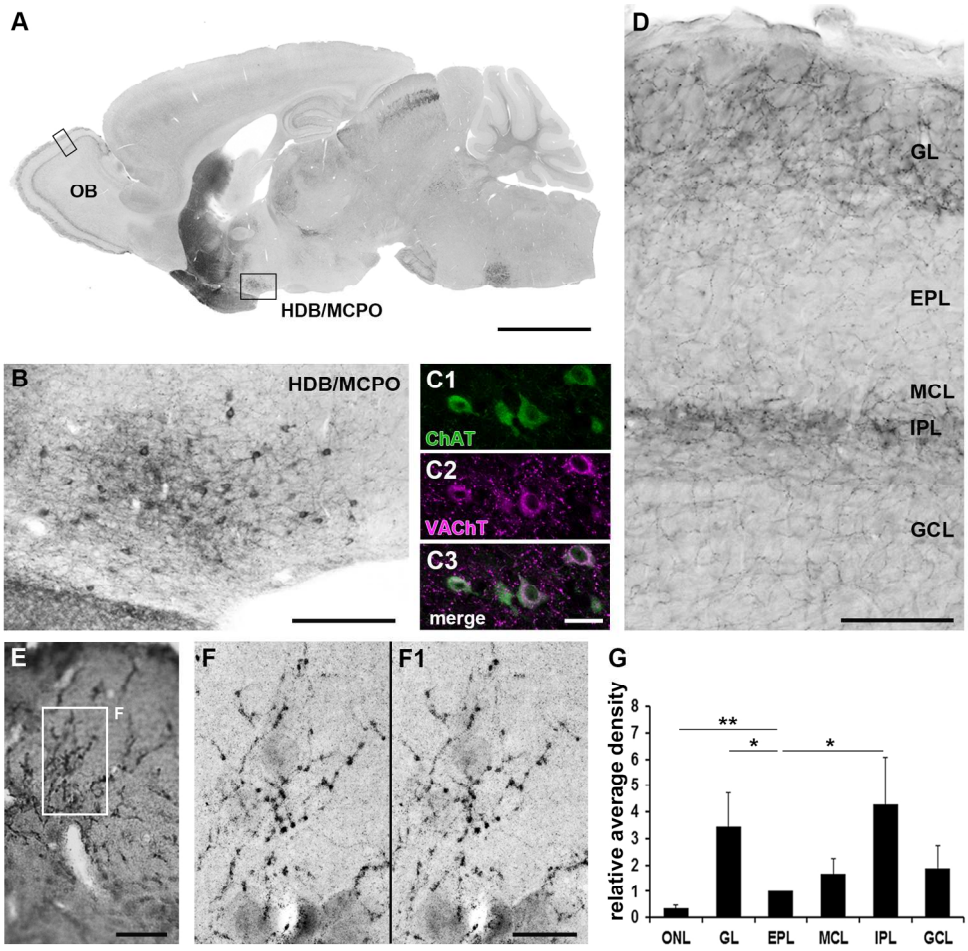

Figure 1. Immunocytochemistry of cholinergic neurons with the anti-VAChT antibody. (A) Cholinergic neurons widely distributed in various brain regions. (B) VAChT-ir somata were found in the HDB/MCPO. (C) Co-expression of ChAT and VAChT in the HDB/MCPO. C1 shows ChAT-ir (green), C2 shows VAChT-ir (magenta), C3 shows the double overlay. (D) Cholinergic fibers were distributed densely in the glomerular layer (GL) and internal plexiform layer (IPL). (E) Light microscopy image for observation of HVEM. (F) A stereo pair of HVEM (± 8°) images showing cholinergic axons in the glomerular and periglomerular regions with branches and varicosities. (G) Quantification of VAChT-ir fiber density was measured by the ROD ratio of each layer to EPL. The majority of fibers were found in the GL and IPL (* $p < 0.05$ and ** $p < 0.01$ compared with EPL). ChAT, choline acetyltransferase; EPL, external plexiform layer; GCL, granule cell layer; HDB, horizontal limb of the diagonal band of Broca; HVEM, high-voltage electron microscopy; -ir, immunoreactive; MCL, mitral cell layer; MCPO, magnocellular preoptic nucleus; ROD, relative optical density; ONL, olfactory nerve layer; VAChT, vesicular acetylcholine transporter. Scale bars = 2 mm in A; 200 μm in B; 50 μm in D; 25 μm in C and E; 10 μm in F.

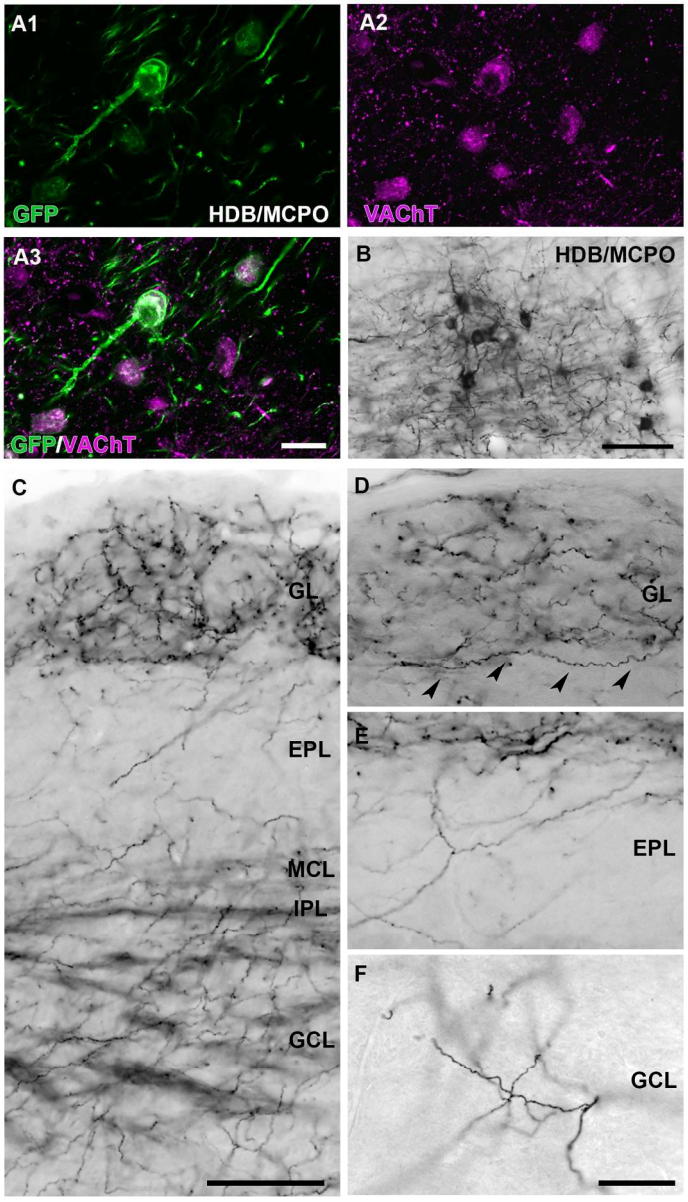

Figure 2. Selective labeling of the cholinergic neuron by viral injection.
(A) Double immunolabeling for characterization of cholinergic neurons in the HDB/MCPO. A1 shows infected neurons (green), A2 shows cholinergic neurons (magenta), and A3 shows the double overlay. All infected neurons in the HDB/MCPO were cholinergic neurons. (B) Fluorescent labeling was converted to bright field labeling in the HDB/MCPO. (C-F) DAB visualization of infected axons in the olfactory bulb. (C) Infected cholinergic fibers were most densely distributed in the glomerular layer (GL). (D) In the GL, the majority of fibers repeatedly branched and crossed into the adjacent glomeruli (arrowheads). (E) In the external plexiform layer (EPL), a small number of fibers which bifurcated were found ascending to the GL. (F) In the granule cell layer (GCL), multiple branching fibers were frequently found. GFP, green fluorescent protein; MCPO, magnocellular preoptic nucleus; HDB, horizontal limb of the diagonal band of Broca. Scale bars = 20μm in A; 100 μm in B and C; 50 μm in F.

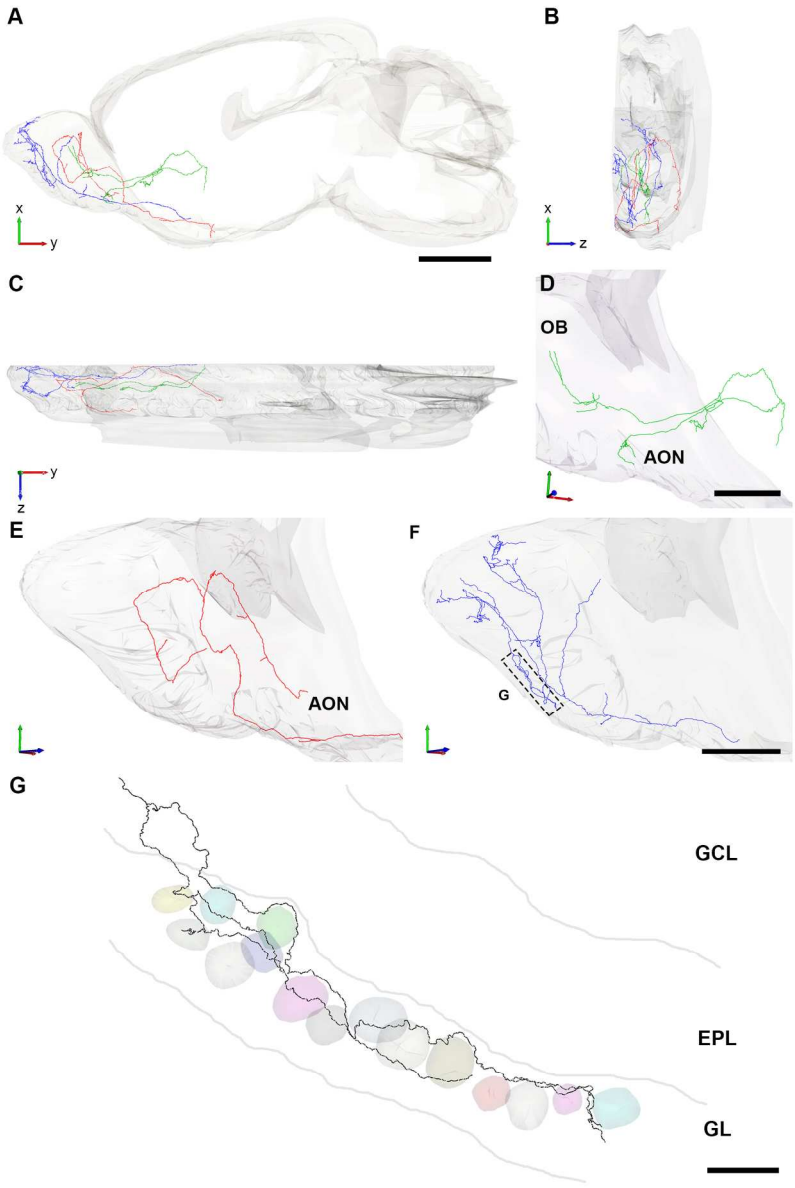

Figure 3. Three-dimensional reconstructions of three cholinergic neurons from the HDB/MCPO to the olfactory bulb (OB). Each cholinergic neuron was reconstructed after infection of ChAT-Cre mice with AAV. (A) Lateral view. (B) Dorsal view. (C) Rostral view. (D) A single axon had branches to the lateral septum nucleus and anterior olfactory nucleus (AON). (E) An axon left the OB and returned to the AON. (F) In the OB, a single axon traveled with multiple ramifications and distributed in both ventral and dorsal sides of the glomerular layer (GL). (G) In the GL, an axon passed through the periglomerular region. Individual glomeruli in the GL are shown in different colors. AAV, adeno-associated virus; ChAT, choline acetyltransferase; HDB, horizontal limb of the diagonal band of Broca; MCPO, magnocellular preoptic nucleus. Scale bars = 2 mm in A (applies B and C); 1 mm in D and F (applies to E); 100 μm in G.

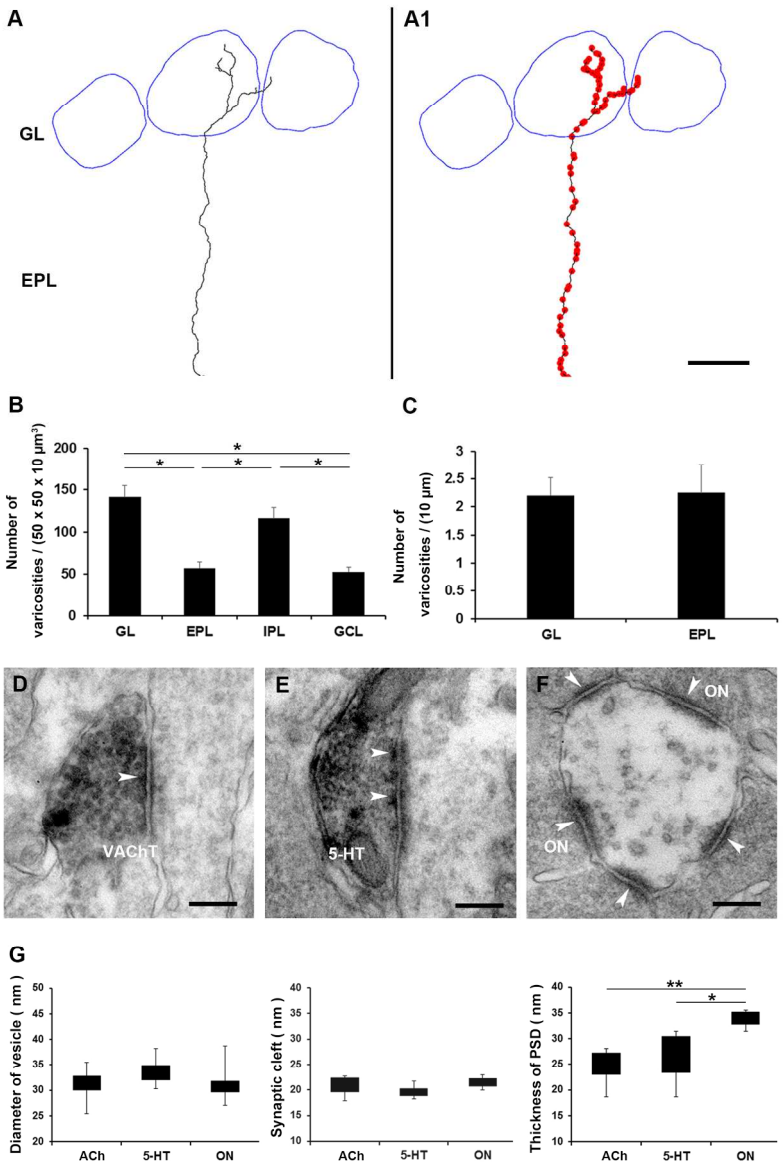

Figure 4. Morphometry of cholinergic neurons and synaptic features.
Reconstruction of a cholinergic axon. The axon ascended vertically from the granule cell layer (GCL) to the glomerular layer (GL). The axon bifurcated four times within the glomeruli, and one of the axonal branches entered into each of the neighboring glomeruli (A, A1; Stereo pairs of 3D reconstruction images ± 8°). A red circle indicates a varicosity. (B) The mean number of varicosities per 50 x 50 x 10 µm3 in each layer. The majority of varicosities were found in the GL and IPL (*p < 0.01 compared with EPL or GCL, Student's t-test). (C) The mean number of varicosities per 10 µm in the GL and the external plexiform layer (EPL). There was no significant difference between the GL and EPL. Electron microscopic images of synapses in the GL (D-F, arrowheads). Synaptic terminals of cholinergic (D), serotonergic (E), and olfactory receptor neurons (F). Morphometry of synaptic vesicles, synaptic cleft, and thickness of PSD (G). There was no statistically significant difference in the synaptic vesicle or synaptic cleft size between the three neurons. There was a statistical difference between the variance of the thickness of PSD of 5-HT neurons and that of olfactory receptor neurons (F = 9.39, p = 0.025, Z-test). Moreover, there was a statistical difference

between the mean of the thickness of the PSDs (Cholinergic vs. ONs; **p < 0.01, student's t-test, Serotonergic vs. ONs; *p < 0.05, Welch test). IPL, internal plexiform layer; MCL, mitral cell layer; ON, olfactory receptor neuron; PSD, postsynaptic density; 3D, three-dimensional; 5-HT, 5-hydroxytryptamine (serotonergic). Scale bars = 50 μm in A; 200 nm in D-F.

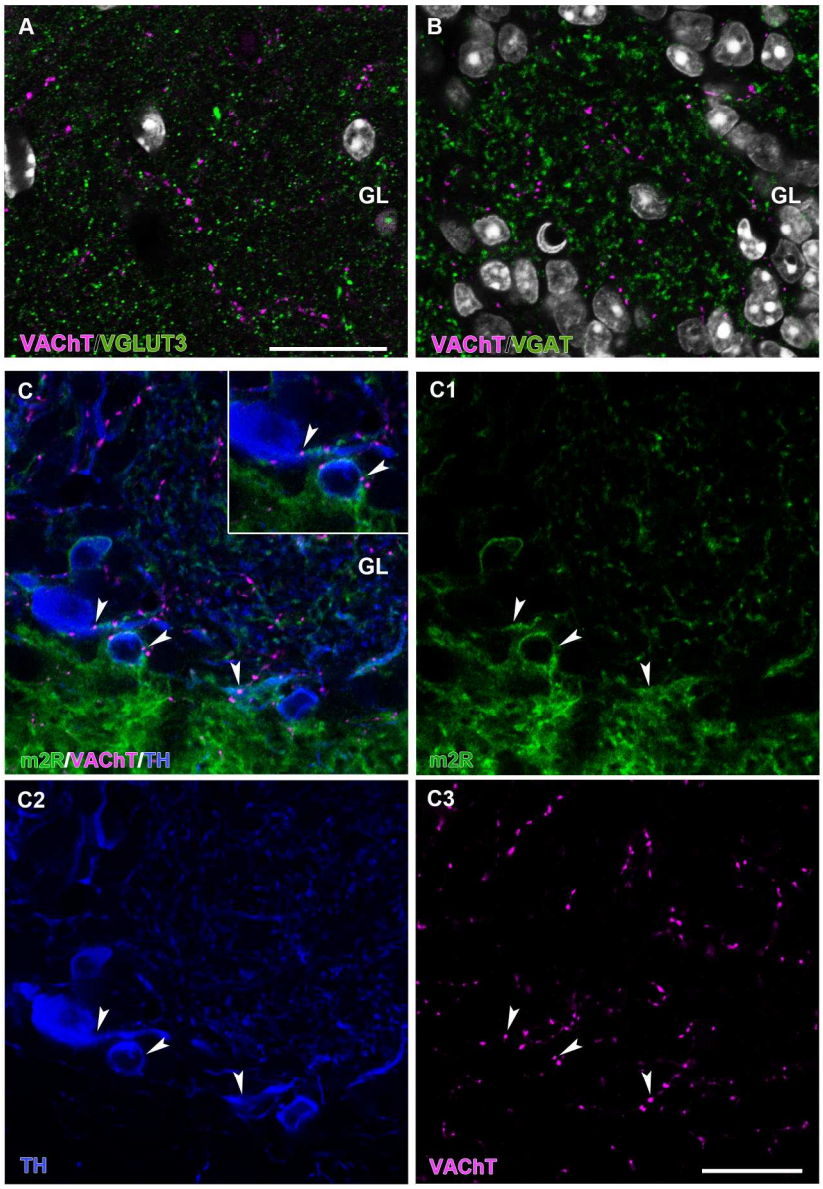

Figure 5. Localization of m2R in the glomerular layer (GL). Double immunostaining shows that VGLUT3 (A) and VGAT (B) were not co-localized in varicosities expressing VAChT. (C) Multiple immunostainings of m2R (green, C1), TH (green, C2), and VAChT (magenta, C3). Expression of m2R was found on TH-ir somata and processes, which are occasionally associated with VAChT-ir varicosities (arrowheads). Most of the m2R-ir puncta did not associate with VAChT-ir. -ir, immunoreactive; m2R, m2 muscarinic acetylcholine receptor; TH, tyrosine hydroxylase; VAChT, vesicular acetylcholine transporter; VGAT, vesicular GABA transporter; VGLUT3, vesicular glutamate transporter 3. Scale bars = 20 μm in B (applies to A) and C.

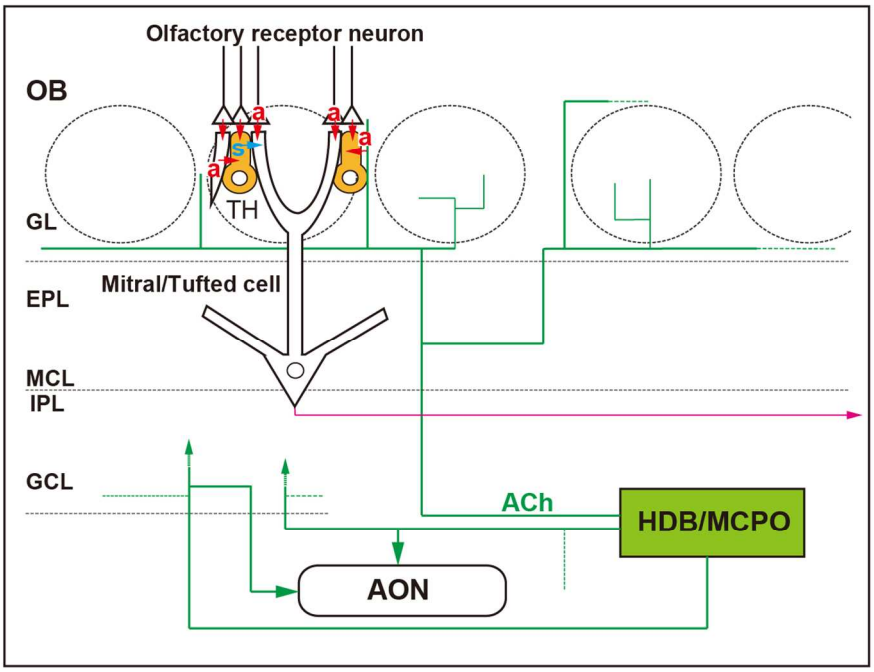

Figure 6. Concluding scheme. Taken together with our previous findings, cholinergic neurons originating from HDB/MCPO project to the OB branching multiple times, distribute to glomeruli localized in different areas of the GL and influence bulbar interneurons.
ACh, acetylcholine; AON, anterior olfactory nucleus; EPL, external plexiform layer; GCL, granule cell layer; GL, glomerular layer; HDB, horizontal limb of the diagonal band of Broca; IPL, internal plexiform layer; MCL, mitral cell layer; MCPO, magnocellular preoptic nucleus; OB, olfactory bulb; TH, tyrosine hydroxylase. a (red), asymmetrical synapse; s (blue), symmetrical synapse.